Stem Cell Reports
Report

ISSCR

OPEN ACCESS

Accumulation of the Vitamin D Precursor Cholecalciferol Antagonizes Hedgehog Signaling to Impair Hemogenic Endothelium Formation

Mauricio Cortes,[1] Sarah Y. Liu,[1] Wanda Kwan,[1] Kristen Alexa,[2] Wolfram Goessling,[2,3] and Trista E. North[1,3,*]
[1]Beth Israel Deaconess Medical Center, Harvard Medical School, Boston, MA 02115, USA
[2]Brigham and Women's Hospital, Harvard Medical School, Boston, MA 02115, USA
[3]Harvard Stem Cell Institute, Harvard University, Cambridge, MA 02138, USA
*Correspondence: tnorth@bidmc.harvard.edu
http://dx.doi.org/10.1016/j.stemcr.2015.08.010

SUMMARY

Hematopoietic stem and progenitor cells (HSPCs) are born from hemogenic endothelium in the dorsal aorta. Specification of this hematopoietic niche is regulated by a signaling axis using Hedgehog (Hh) and Notch, which culminates in expression of Runx1 in the ventral wall of the artery. Here, we demonstrate that the vitamin D precursor cholecalciferol (D3) modulates HSPC production by impairing hemogenic vascular niche formation. Accumulation of D3 through exogenous treatment or inhibition of Cyp2r1, the enzyme required for D3 25-hydroxylation, results in Hh pathway antagonism marked by loss of Gli-reporter activation, defects in vascular niche identity, and reduced HSPCs. Mechanistic studies indicated the effect was specific to D3, and not active 1,25-dihydroxy vitamin D3, acting on the extracellular sterol-binding domain of Smoothened. These findings highlight a direct impact of inefficient vitamin D synthesis on cell fate commitment and maturation in Hh-regulated tissues, which may have implications beyond hemogenic endothelium specification.

INTRODUCTION

Hematopoietic stem cells (HSCs) have the lifelong ability to self-renew and generate each of the blood lineages. In vertebrates, definitive hematopoiesis begins with de novo birth of HSCs from hemogenic endothelium along the ventral wall of the dorsal aorta in a conserved region known as the aorta-gonad-mesonephros (AGM) (Dzierzak and Medvinsky, 2008). Studies in zebrafish and mammals have demonstrated that formation of the hematovascular niche is dependent on a signaling cascade between the Hedgehog (Hh) and the Notch pathways. This signaling controls placement of the stem cell leukemia (SCL) transcription factor and induction of the first definitive HSC marker, Runx1 (Gering and Patient, 2005; Kim et al., 2013; Lawson et al., 2002). Based on the conserved role of *runx1* in zebrafish (Burns et al., 2005; Kissa and Herbomel, 2010; North et al., 2002), we previously performed a chemical screen to identify regulators of HSC production (North et al., 2007). We recently showed cholesterol-derived estrogens have a crucial role in establishing hemogenic endothelium boundaries (Carroll et al., 2014); the cholesterol derivative vitamin D was likewise identified as a candidate hematopoietic stem and progenitor cell (HSPC) regulator in the screen.

Vitamin D synthesis begins with the transformation of 7-dehydrocholesterol in the skin by UV radiation to generate the non-active vitamin D precursor cholecalciferol (D3). Some vertebrates, including teleosts (e.g., zebrafish), obtain D3 primarily from their diet (Lock et al., 2010). D3 is modified by the cytochrome P450 enzyme 2R1 (CYP2R1) to generate 25-hydroxy vitamin D (25(OH)D3), the circulating form of vitamin D, which is then further hydroxylated by CYP27B1 to generate the active vitamin D metabolite, 1,25-dihydroxy vitamin D3 (1,25(OH)D3). Active 1,25(OH)D3 functions as the ligand for the vitamin D receptor (VDR), a member of the nuclear hormone receptor family, resulting in nuclear localization and transcriptional regulation (Plum and DeLuca, 2010). Ligand binding also induces non-genomic cellular responses, including calcium uptake (Norman, 2006). Zebrafish exhibit strong conservation of the vitamin D biosynthetic pathway and its downstream signaling cascade (Craig et al., 2008; Lin et al., 2012).

Beyond the established role of 1,25(OH)D3 in VDR signaling, the biological function of vitamin D precursors in mediating non-VDR dependent events remains controversial. Mutations in 7-dehydrocholesterol reductase are associated with Hh defects in mammals (Koide et al., 2006). Cell culture studies designed to isolate cholesterol derivatives affecting Hh signaling identified 3beta-hydroxysteroids, including D3, as negative Hh regulators in C3H/10T1/2 fibroblasts (Bijlsma et al., 2006). This study and others indicated exogenous addition of D3 may block Hh activity in a VDR-independent manner, potentially at the level of Smoothened (Bijlsma et al., 2006; Tang et al., 2011). Beyond these preliminary analyses, the mechanism of action of potential D3-mediated Hh regulation remains unclear and in vivo physiological relevance has not been elucidated.

Here, we demonstrate that exposure to elevated D3 (12–24 hours post fertilization [hpf]) negatively regulates hematovascular niche specification, decreasing HSPC numbers while sparing the gross development of the dorsal aorta. D3

inhibits the Hh signaling axis via binding in vivo to the recently described extracellular sterol-binding domain of Smoothened. Likewise, physiological accumulation of D3 mediated by inhibition of *cyp2r1* significantly reduced Hh activity and disrupted hemogenic niche specification, leading to low HSPCs. Together, these in vivo studies indicate inefficient vitamin D synthesis affects cellular specification and tissue maturation in the embryo, independent of reductions in 1,25(OH)D3 content, via negative regulation of the Hh signaling pathway.

RESULTS

Vitamin D Metabolites Differentially Regulate Definitive Hematopoiesis

Vitamin D was isolated in a prior chemical screen in zebrafish as a potential modulator of HSPC gene expression (North et al., 2007). To characterize the impact of vitamin D on definitive hematopoiesis, zebrafish embryos were exposed to the non-hydroxylated vitamin D precursor D3 and the active hydroxylated vitamin D metabolite, 1,25(OH)D3, between 12 and 36 hpf during the onset of HSPC formation. Treatment with D3 decreased expression of conserved HSPC markers *runx1* and *cmyb* as determined by whole-mount in situ hybridization (WISH) at 36 hpf (Figures 1A and 1B) and reduced HSPC-reporter (*Tg(runx1P2:eGFP)*) activity in the AGM (Figure 1C). In contrast, 1,25(OH)D3 increased both *runx1/cmyb* expression and Runx1 reporter activity (Figures 1A–1C), suggesting distinct modes of action. To confirm and quantify these findings, fluorescence-activated cell sorting (FACS) analysis was performed using *Tg(lmo2:dsRed);Tg(cmyb:gfp)* embryos, highlighting a broad population of HSPCs: D3 caused a 25% ($p < 0.01$) decrease, while 1,25(OH)D3 elicited a 20% ($p < 0.01$) increase in HSPC numbers (Figure 1D). To elucidate the cause of the differential regulation, embryos were treated for select intervals during hemogenic vascular endothelium specification (12–24 hpf) or definitive HSPC production (24–36 hpf). Whereas 1,25(OH)D3 increased *runx1/cmyb* WISH expression during either treatment window, the negative effect of D3 was predominantly observed with exposure between 12 and 24 hpf (Figures 1E and 1F). qPCR confirmed that statistically significant reductions in *runx1* were seen only after early D3 treatment, indicative of an effect on the HSPC niche (Figure S1A). However, analysis of *flk1* expression indicated vasculogenesis was not grossly altered (Figure S1B). Early D3 exposure also had a minimal effect on the expression of *cyp24a1*, a direct VDR transcriptional target, while 1,25(OH)D3 was a potent activator (Figure S1C). Together, these data suggest D3 affects HSPC production via VDR-independent alterations in vascular niche specification.

D3 Exposure Inhibits Hh-Notch-Mediated Hemogenic Niche Specification

In vertebrates, HSCs are born from hemogenic endothelium specified by highly orchestrated signaling events starting with the Hh pathway and ending with Notch activity (Carroll et al., 2014; Kim et al., 2013; Lawson et al., 2002). Based on this pivotal role in vascular niche specification and prior studies describing potential inhibitory effects of D3, we hypothesized that D3 accumulation affected HSPC formation via inhibition of the Hh-Notch signaling cascade. To determine whether D3 could act to antagonize Hh-regulated developmental processes in vivo, the *Tg(gli-d:mcherry)* reporter line was used (Schwend et al., 2010). D3-treated embryos showed reduced Gli-reporter activity in the trunk region as determined by WISH (Figures 2A and 2B), similar to that seen with the Hh inhibitor cyclopamine. Co-treatment caused more severe inhibition, suggesting synergistic Hh antagonism (Figures 2A and 2B). FACS analysis of whole embryo disaggregates revealed a 54% ($p < 0.01$) decrease in total Gli-reporter-positive cells by D3 treatment alone and a 91% ($p < 0.001$) loss in combination with cyclopamine (Figure 2C). In contrast, no reduction in Hh activity was observed following 1,25(OH)D3 treatment by Gli-reporter WISH or FACS (Figures S2A and S2B). To confirm the effect of D3 was independent of VDR signaling, a previously validated morpholino (MO) was employed (Lin et al., 2012). No significant changes in Gli-reporter expression were seen with *vdra* knockdown (Figures S2C and S2D); however, morphants exposed to D3 still had reduced Hh activity (Figure 2D), supporting an alternate mechanism of action.

Consistent with a role for Hh upstream of Notch in vascular specification, D3 also diminished Notch-reporter activity (*Tg(EPV.Tp1CMmu.Hbb:EGFP)*) in the trunk vessels by WISH (Figures 2E and 2F), which was exacerbated by cyclopamine. D3-treated embryos had an expanded region of venous identity marked by *flt4* and concomitant decreases in arterial fate as indicated by *ephrinb2a* (Figure S2E), consistent with published reports (Lawson et al., 2002; Carroll et al., 2014). Reductions in arterial *ephrinb2a* and *notch3* (Figure S2F), and the Hh target *ptc1*, with D3 exposure were confirmed by qRT-PCR. In contrast, neither addition of 1,25(OH)D3 nor *vdra* MO affected vascular niche and Hh target expression (Figures S2G and S2H). Finally, *scl*+ hemogenic endothelium was profoundly lost in D3-treated embryos (Figures 2G and 2H), confirming disruption of the most proximal specification event downstream of Hh-Notch signaling to HSPCs.

20(S)-OHC Rescues D3-Mediated Inhibition of Smoothened and Hh Activity

The G-coupled protein receptor Smoothened was previously identified as the target of cyclopamine-mediated

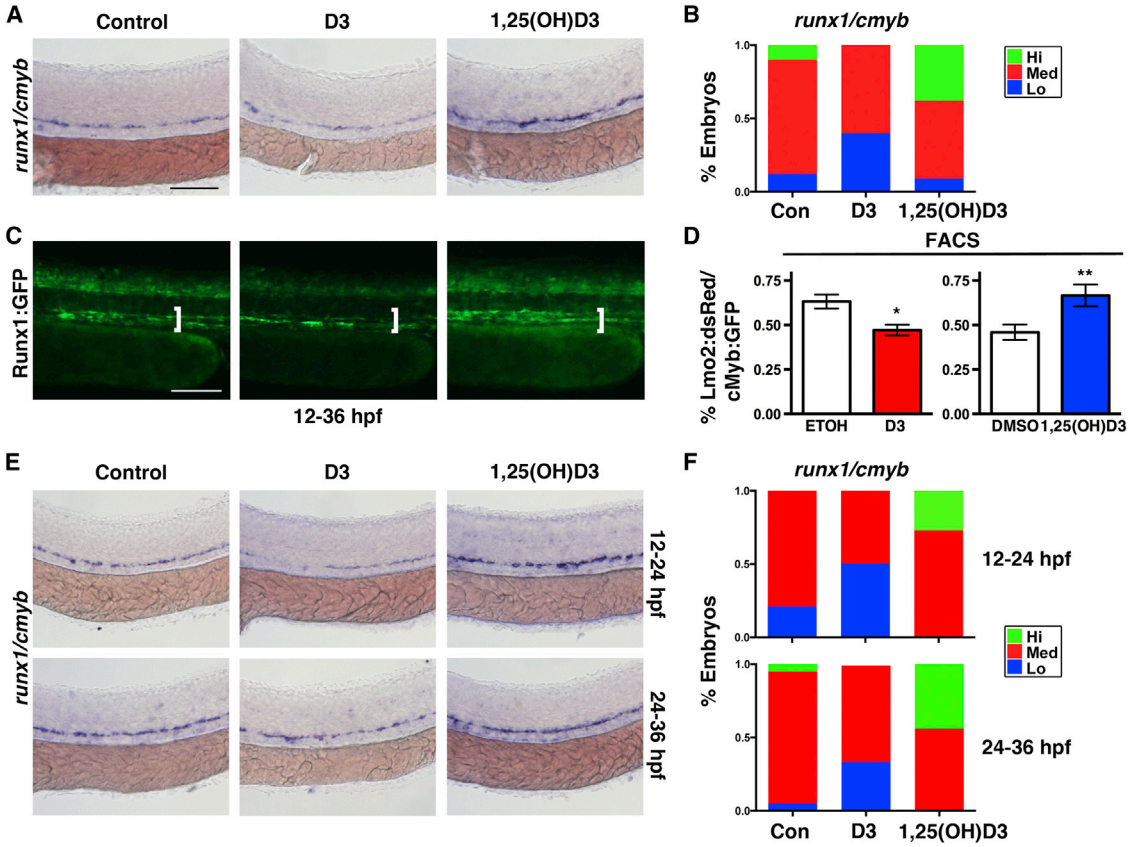

Figure 1. Vitamin D Metabolites Have Differential Effects on HSC Formation

(A) Exposure to D3 (50 μM) decreased *runx1/cmyb* expression by WISH at 36 hpf, and 1,25(OH)D3 (10 μM) increased expression. Scale bar, 100 μm.

(B) Qualitative phenotypic distribution of embryos from (A) scored with low, medium, or high *runx1/cmyb* expression in the AGM (n > 50 embryos/condition).

(C) Runx1:GFP embryos exhibited either diminished or enhanced expression with D3 or 1,25(OH)D3 exposure, respectively. Scale bar, 100 μm.

(D) FACS analysis of double-positive HSPCs in Lmo2:dsRed/cMyb:GFP embryos confirmed a 25% (*p = 0.014) decrease with D3 versus a 20% (**p = 0.029) increase with 1,25(OH)D3 compared to controls (5 embryos/sample × 4 replicates/condition). Error bars, mean ± SD.

(E) D3 treatment during hemogenic niche specification (12–24 hpf) or HSC induction (24–36 hpf) only decreased *runx1/cmyb* by WISH in the early exposure window, whereas 1,25(OH)D3 increased expression during either treatment period. Scale as in (A).

(F) Qualitative phenotypic distribution of embryos from (E) scored for *runx1/cmyb* as in (B) (n > 20 embryos/condition).

See also Figure S1.

Hh pathway inhibition; prior in vitro data suggested D3 may antagonize the same target (Bijlsma et al., 2006). Oxysterols, which stimulate Hh signaling (Corcoran and Scott, 2006), were recently shown to bind in the extracellular cysteine-rich domain (CRD) of Smoothened, distinct from the heptahelical pocket cyclopamine targets (Nedelcu et al., 2013). To elucidate the mechanism of action of D3 on Hh activity in vivo, D3-treated embryos were exposed to Smoothened agonists SAG and 20(S)-hydroxycholesterol (20(S)-OHC) (Figure 3A). SAG binds to the heptahelical bundle, and can directly compete with cyclopamine (Chen et al., 2002), whereas 20(S)-OHC binds the N-terminal extracellular CRD (Nedelcu et al., 2013). Co-treatment with SAG failed to block D3-mediated Hh inhibition as seen by Gli-reporter FACS (Figure 3B). In contrast, exposure to 20(S)-OHC preserved Hh signaling in the presence of D3 ($p < 0.05$) (Figure 3B). Co-exposure to 20(S)-OHC also restored *ptc2* and *runx1* expression in D3-treated embryos by qRT-PCR ($p < 0.005$) (Figure 3C), as well as HSPC induction by WISH (Figures 3D and 3E). These data indicate D3 inhibits Hh-dependent hemogenic endothelium specification in vivo by interactions with the Smoothened CRD.

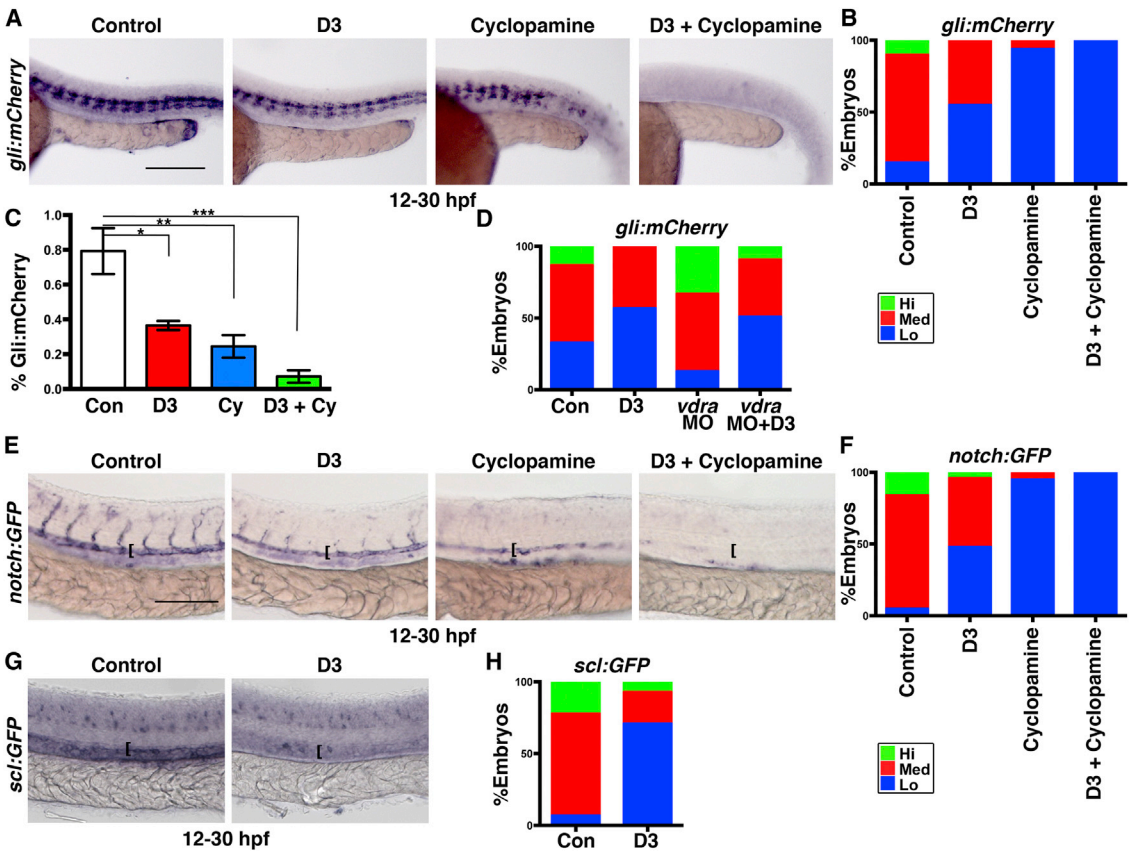

Figure 2. D3 Negatively Regulates Hh-Mediated Vascular Niche Specification

(A) Gli:mCherry expression was decreased in D3-treated embryos compared to controls by WISH. Cyclopamine co-treatment caused synergistic reduction. Scale bar, 200 μm.

(B) Qualitative phenotypic distribution of embryos from (A) scored for *gli:mcherry* (n > 20 embryos/condition).

(C) Gli:mCherry FACS showed significant decreases in Hh responsive cells in D3 (54%, *p = 0.006), cyclopamine (70%, **p = 0.001), or co-treated embryos (91%,***p = 0.001) (5 embryos/sample × 4 replicates/condition). Error bars, mean ± SD.

(D) Qualitative phenotypic distribution of *gli:mcherry* expression in *vdra* morphants occurred in the presence or absence of D3 treatment (n > 20 embryos/condition).

(E) D3 reduced Notch reporter activity in intersomitic and axial vessels, similar to cyclopamine, by WISH. Co-treatment exacerbated Notch inhibition. Scale bar, 100 μm.

(F) Qualitative phenotypic distribution of embryos from (D) scored for *Notch-GFP* (n > 20 embryos/condition).

(G) SCL-GFP embryos treated with D3 (12–30 hpf) had reduced *scl*+ hemogenic endothelium by WISH for GFP. Scale as in (E).

(H) Qualitative phenotypic distribution of embryos from (F) scored for *scl:GFP* (n > 10 embryos/condition).

See also Figure S2.

Loss of *cyp2r1* Negatively Affects Hh Activity via D3/Smoothened Antagonism

Vitamin D synthesis begins concurrently with the onset of definitive hematopoiesis, as *cyp2r1* (25-hydroxylase), *cyp27b1* (1-hydroxylase), and *cyp24a1* (24-hydroxylase) are actively transcribed in the embryo by 24 hpf (Figure S3A). Mutations in *CYP2R1*, which catalyzes the first hydroxylation step in the enzymatic processing of D3 to 1,25(OH)D3, are associated with human vitamin D deficiency. To determine the potential physiological relevance of *cyp2r1* mutation-mediated D3 accumulation on Hh-dependent hematovascular specification, embryos deficient in *cyp2r1* were created by the clustered regularly interspaced short palindromic repeat (CRISPR)-CRISPR-associated 9 (Cas9) system (Jao et al., 2013). An allele with a 25-base pair deletion in exon 3, predicted to encode a truncated protein with a severely compromised active site, was produced (Figures S3B and S3C). Targeted deletion of *cyp2r1* diminished *runx1* expression (50% penetrance) compared to sibling controls (Figure 4A) while leaving *flk1*+ vasculature grossly normal (Figure 4B). To confirm and quantify these observations, a *cyp2r1* MO

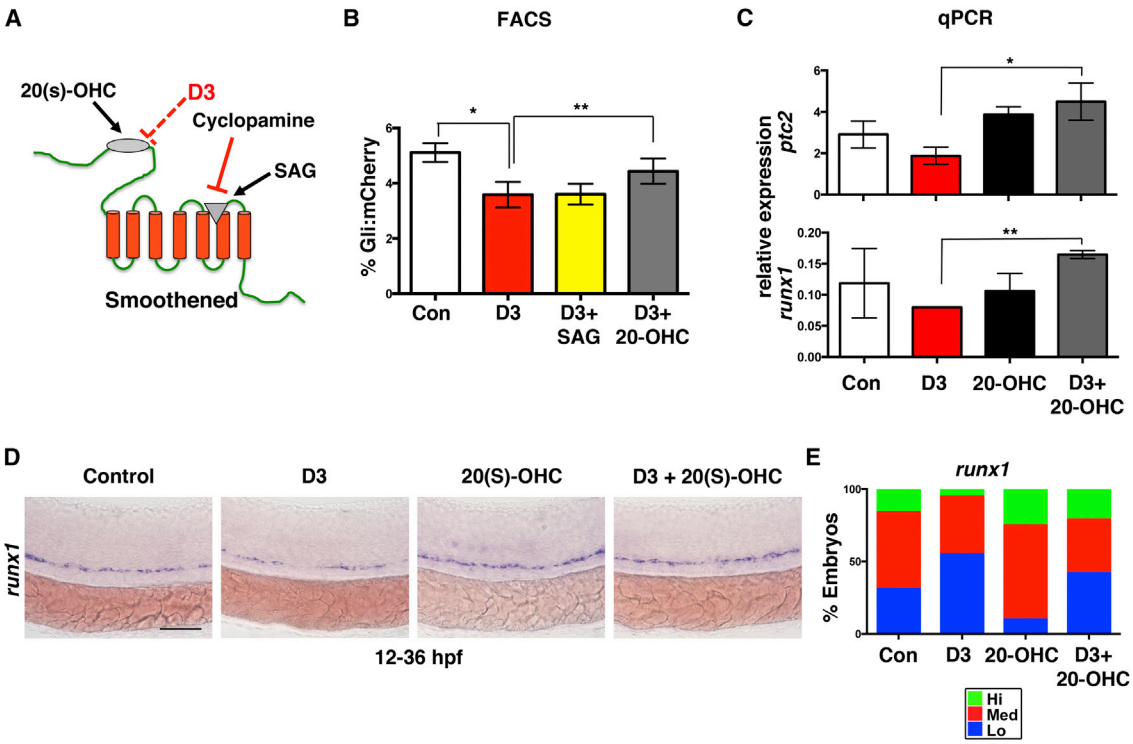

Figure 3. D3 Antagonizes Hh Signaling via Interaction with the Extracellular Domain of Smoothened

(A) Diagram depicts the sites of action of Hh pathway modifiers cyclopamine, SAG, and 20-OHC on the Smoothened receptor. The presumptive site of D3 action (red) is shown.

(B) FACS of Gli-reporter embryos showed D3 decreased Hh activity (*p = 0.002). SAG co-treatment (5 μM) did not alter the effect of D3, while 20(S)-OHC (10 μM) partially blocked Hh inhibition (**p = 0.040) (5 embryos/sample × 4 replicates/condition). Error bars, mean ± SD.

(C) Co-treatment with 20(S)-OHC corrected D3-mediated reductions in *ptc2* (*p = 0.019) and *runx1* (**p = 0.003) by qPCR (40 pooled embryos/condition × 3 replicates). Error bars, mean ± SD.

(D) 20(S)-OHC restored *runx1* expression in D3-treated embryos. Scale bar, 100 μm.

(E) Qualitative phenotypic distribution of embryos from (D) scored for *runx1* (n > 20 embryos/condition).

was employed (Figures S3D and S3E). Morphants had a similar decrease in *runx1/cmyb* expression to that of *cyp2r1* mutants (Figures 4C and 4D), with FACS indicating a 21% ($p < 0.05$) reduction in Flk1:dsRed+/cMyb:GFP+ HSCs (Figure 4E). Consistent with diminished Hh signaling due to D3 accumulation, *cyp2r1* mutants exhibited substantially reduced *ptc2* expression (77% penetrance) (Figure 4F). These effects were validated by Gli-reporter WISH following *cyp2r1*-MO knockdown (Figures 4G and 4H) and quantified as a 33% ($p < 0.01$) decrease in Hh activity by FACS (Figure 4I). The *cyp2r1* morphants also had reduced Notch-reporter activity (Figures S4A and S4B) and artery or vein defects (Figures S4C and S4D), as seen with D3 exposure. In contrast, no inhibitory effect was seen in embryos injected with a MO to *cyp27b1* (Figures S4E–S4G), further indicating that D3 accumulation, rather than loss of 1,25(OH)D3, caused the Hh phenotypes. To confirm the specificity of Cyp2r1 function in Hh regulation, morphants were co-injected with full-length zebrafish *cyp2r1* mRNA, mitigating the Gli-reporter phenotype (Figure 4J). Finally, to corroborate Smoothened antagonism, as found for D3, morphant embryos were treated with 20(S)-OHC and Gli-reporter activity was restored (Figure 4K). In sum, these data show that physiologically relevant reductions in vitamin D biosynthesis, occurring at the level of D3 hydroxylation via *cyp2r1* mutation, negatively affect Hh-dependent processes like hematovascular specification in vivo by accumulation of D3 and direct inhibition of the Smoothened CRD.

DISCUSSION

Beyond the role of vitamin D in calcium homeostasis, severe vitamin D deficiency in humans is associated with a variety of hematopoietic disorders, including anemia and

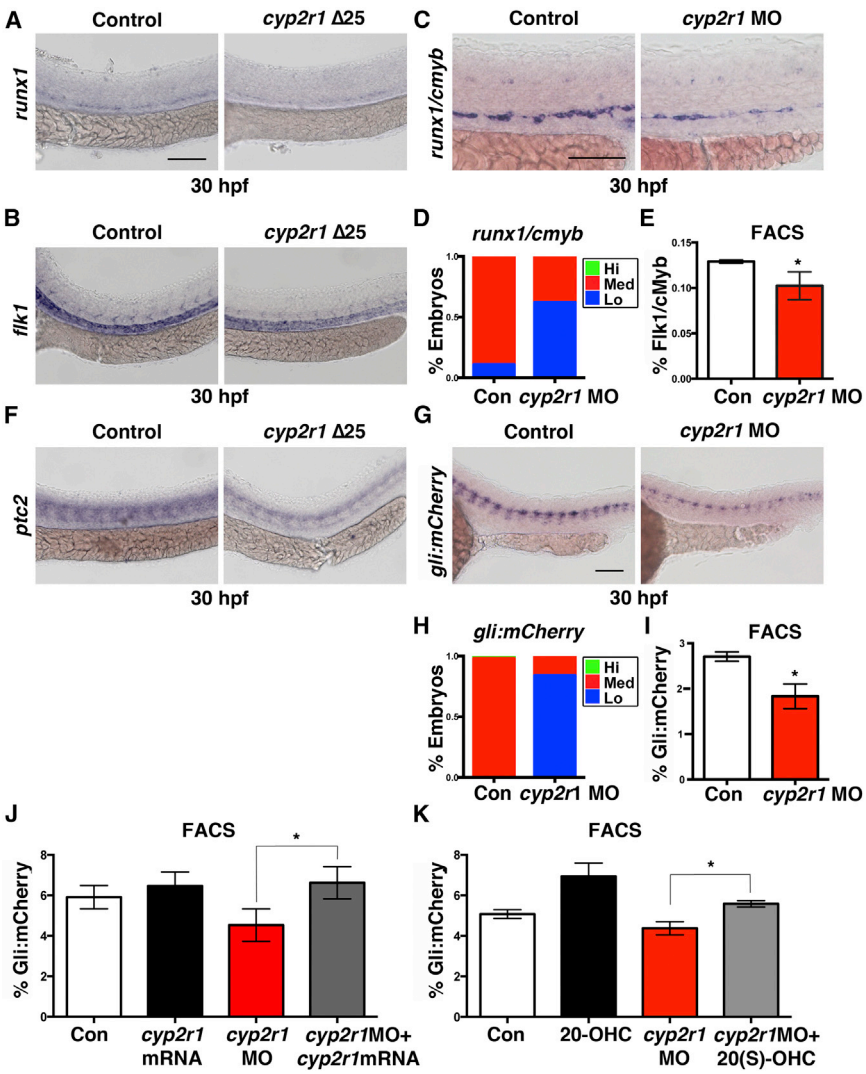

Figure 4. Cyp2r1 Inhibition and Failed D3 Hydroxylation Elicits Hh-Related Defects in HSPC Production

(A) WISH for *runx1* showed *cyp2r1* mutation results in HSPC defects. Scale bar, 100 μm.

(B) WISH for *flk1* revealed minimal impact of *cyp2r1* loss on trunk vessels. Scale as in (A).

(C) *cyp2r1* morphants had diminished *runx1/cmyb* expression. Scale bar, 50 μm.

(D) Qualitative phenotypic distribution of embryos from (C) scored for *runx1* (n > 30 embryos/condition).

(E) Flk:dsRed+/cMyb:GFP+ FACS indicated a 21% (*p = 0.0328) decrease in HSCs in *cyp2r1* morphants (5 embryos/sample × 4 replicates/condition). Error bars, mean ± SD.

(F) In *cyp2r1* mutants, *ptc2* WISH showed Hh signaling was affected by endogenous D3 accumulation (77% penetrance). Scale as in (A).

(G) WISH for Gli-reporter expression in *cyp2r1* morphants confirmed low Hh activity was correlated with ineffective D3 hydroxylation. Scale bar, 100 μm.

(H) Qualitative phenotypic distribution of embryos from (G) scored for *mcherry* expression (n > 40 embryos/condition).

(I) FACS of *cyp2r1*-MO-injected Gli-reporter embryos revealed a 33% (*p = 0.0065) decrease in Hh activity (n value and error bars as in E).

(J) Gli:mCherry FACS showed co-injection of zebrafish *cyp2r1* mRNA-rescued, *cyp2r1*-MO-meditated decreases in Hh activity (*p = 0.009) (n value and error bars as in E).

(K) 20(s)-OHC-rescued defects in Hh activity caused by *cyp2r1* knockdown as shown by FACS of the Gli-reporter line (*p = 0.0005) (n value and error bars as in E).

See also Figures S3 and S4.

extramedullary hematopoiesis (Yetgin et al., 1989), due to alterations in the bone marrow microenvironment. *VDR*-deficient mice likewise display extramedullary hematopoiesis (Jeanson and Scadden, 2010). Vitamin D is also important in the immune system, specifically affecting T cell development and function (Kongsbak et al., 2013). Despite these findings, there is minimal investigation into the role of vitamin D regulation in the earliest stages of hematopoiesis. In this study, we demonstrate that vitamin D precursor D3 affects hemogenic vascular niche specification, affecting HSPC numbers during embryogenesis. Excess D3 derived from exogenous exposure or insufficient Cyp2r1 function diminished Hh signaling and disrupted Hh-regulated mesodermal cell fate. Significantly, these effects were not phenocopied by 1,25(OH) D3 or dependent on VDR activity. Rather, our data indicate that D3 acts directly on Smoothened at the recently defined extracellular sterol-binding domain (Figure 3A). The strong synergy observed between D3 and cyclopamine toward Hh inhibition in vivo is consistent with prior mechanistic studies in which 20(S)-OHC and SAG mediated allosteric interactions between the CRD and the heptahelical binding domains of Smoothened to result in maximum pathway activation (Nachtergaele et al., 2012). Finally, the *cyp2r1* loss-of-function studies demonstrate a physiological role for D3 in Hh pathway inhibition. These findings are intriguing in the context of human disease, because *CYP2R1* mutations result in vitamin D-deficient rickets marked by skeletal abnormalities, with low levels of 25(OH)D3 but relatively normal

levels of 1,25(OH)D3 (Al Mutair et al., 2012). While it has been postulated that maintenance of 1,25(OH)D3 sufficiency is due to increased parathyroid hormone activity and alterations in *CYP27B1* and *CYP24A1* function, it will be important to re-evaluate whether developmental abnormalities in these patients are partially due to reductions in Hh signaling caused by D3 accumulation. It will also be interesting to examine interplay between abnormal vitamin D biosynthesis and Hh signaling in cancer, specifically in tissues where both pathways intersect. In summary, we elucidated the physiological consequences of abnormal vitamin D biosynthesis at the level of D3 hydroxylation on hematovascular specification and characterized the mechanism of action in vivo as an antagonistic interaction of D3 with Smoothened and the Hh signaling pathway.

EXPERIMENTAL PROCEDURES

Zebrafish Husbandry

Zebrafish were maintained in accordance with the Beth Israel Deaconess Medical Center Institutional Animal Care and Use Committee. The following lines were used: AB, Tuebingen, *cyp2R1* mutant, *Tg(lmo2:dsred)* (Zhu et al., 2005), *Tg(cmyb:eGFP)* (North et al., 2007), *Tg(flk1:dsRed2ex)* (Kikuchi et al., 2011), *Tg(runx1P2:eGFP)* (Lam et al., 2009), *Tg(Gli-d:mCherry)* (Schwend et al., 2010), and *Tg(EPV.Tp1CMmu.Hbb:EGFP)* (Parsons et al., 2009).

Chemical Treatments

Zebrafish embryos were exposed to chemical modulators in E3 fish medium from 12 to 36 hpf in multi-well plates. The following compounds were used: D3 (50 μM, Enzo), 1,25(OH)D3 (10 μM, Cayman Chemical), cyclopamine (50 μM, LC Laboratories), 20(S)-OHC (10 μM, Tocris), and SAG (10 μM, Tocris). Treated embryos were analyzed by WISH using previously published probes to *runx1*, *cmyb*, *flk1*, *gfp*, *flt4*, *ephrinb2a*, and *ptc2* (Carroll et al., 2014) and established methods (https://zfin.org/ZFIN/Methods/ThisseProtocol.html). Data were qualitatively analyzed and graphically depicted as the percentage falling into each of three phenotypic expression bins. "Medium" expression was set as the most representative phenotype in the normal bell-curve distribution of each cohort of controls ($n \geq 3$ replicate clutches). Images were acquired using a Zeiss Axio Imager A1/AxioCam MRc using AxioVision LE software.

MO and mRNA Injections

MOs (Gene Tools) were injected at the one-cell stage: *cyp2r1*MO1-5′-TGATCGATATCATCTTAGATGCAAA-′3, *cyp2r1*MO2-5′-TTCCATAAGGAACCACTTACCTCCC-3′, *cyb27b1*MO-5′-TGAAGCACCATCATCATCCTCCTGC-3′, and *vdra*MO-5′-ACGGCACTATTTTCCGTAAGCATCC-3′. Splicing efficiency of the *cyp2r1* MO was determined by qRT-PCR using the following primer set: Cyp2r1Fwd-5′-ATGATATCGATCAAACGCTTAACATCACCG-3′ and Cyp2r1Rev-5′-CAGAAATCCTCACAAACATCCTCCGCTGGC-3′. Specificity was tested by injection of in vitro transcribed full-length *cyp2r1* mRNA (100 ng/μl). Synthesis was performed using mMessage mMachine T7 and the Poly(A) Tailing Kit (Life Technologies).

Embryo Dissociation and FACS Analysis

Fluorescent embryos (5 embryos/sample × 4 replicates/condition) were incubated in 0.5 mg/ml of Liberase (Roche) with gentle agitation at 37°C for 2 hr and then manually dissociated by pipetting, filtered, washed, and resuspended in 1× PBS. Samples were treated with SYTOX Red dead cell stain (5 nM, Life Technologies) and analyzed using a BD Biosciences FACSCanto II and LSRII 5 SORP. Data were processed on Flojo X software (Tree Star), and statistics (two-tailed Student's t test) were performed using Prism 6 (GraphPad).

qRT-PCR Performance

Total RNA (40 pooled embryos/condition) was purified using the RNAqueous Total RNA isolation kit, followed by DNase-I treatment, and used to generate cDNA using the Superscript III First Strand Synthesis Supermix (Life Technologies). qRT-PCR was performed using SYBR Green PCR Master Mix (Life Technologies) on a Bio-Rad CFX384. Samples were run in triplicate with >2 biological replicates/condition using primer sequences in Table S1. RT-PCR Miner (http://ewindup.info/miner/) was used for analysis, with statistics as explained earlier.

Cyp2r1 Mutation Generation and Validation

Guide RNA (gRNA) targeting *cyp2r1* was designed using Zifit Targeter (http://zifit.partners.org). Oligos to the *cyp2r1* gRNA sequence 5′-GGACTTCTGAACTGCAAATA-3′ were annealed, cloned into pT7-gRNA (Addgene #46759), and in vitro transcribed using MEGAshortscript-T7 (Life Technologies). Cas9 RNA (100 ng), transcribed from pT3Ts-nls-zCas9-nls (Addgene #46757) using mMessage mMachine T3, as explained earlier, was co-injected with gRNA-*cyp2r1* (50 ng) at the one-cell stage and raised to adulthood. *cyp2r1*-F1 mutants were identified by PCR amplification flanking the target sequence: Cyp2r1CrispF-5′-ATTGCTGTTTGACCAGTCATCCCTGATCGA-3′, Cyp2r1CrispR-5′-CAGGGGAAGGCGTTGTACAGGAAAGCCCAA-3′, and EagI (NEB) restriction digest. DNA sequencing confirmed the mutant *cyp2r1* allele.

SUPPLEMENTAL INFORMATION

Supplemental Information includes a Supplemental Experimental Procedures table, four figures, and can be found with this article online at http://dx.doi.org/10.1016/j.stemcr.2015.08.010.

AUTHOR CONTRIBUTIONS

M.C. designed, performed, and analyzed all experiments. S.Y.L. performed MO injections and WISH. W.K. conducted embryo treatments and qPCR. K.A. provided *cyp24a1*, *cyp2r1*, and *cyp27* plasmids. W.G. provided guidance and edited the manuscript. T.E.N. guided the project and composed the manuscript with M.C.

ACKNOWLEDGMENTS

We thank S. Alhgren (*Tg(Gli-d:mCherry)*), N. Lawson (*Tg(EPV.Tp1CMmu.Hbb:EGFP)*), and P. and K. Crosier (*Tg(Runx1P2:eGFP)*) for transgenic lines; S. Wente and W. Chen for CRISPR-Cas9 plasmids; and the BIDMC Flow Cytometry Core for technical assistance. This study was supported by a V-Foundation Scholar Award (T.E.N.) and the Harvard Stem Cell Institute (T.E.N.).

Received: April 22, 2015
Revised: August 8, 2015
Accepted: August 8, 2015
Published: September 10, 2015

REFERENCES

Al Mutair, A.N., Nasrat, G.H., and Russell, D.W. (2012). Mutation of the CYP2R1 vitamin D 25-hydroxylase in a Saudi Arabian family with severe vitamin D deficiency. J. Clin. Endocrinol. Metab. *97*, E2022–E2025.

Bijlsma, M.F., Spek, C.A., Zivkovic, D., van de Water, S., Rezaee, F., and Peppelenbosch, M.P. (2006). Repression of smoothened by patched-dependent (pro-)vitamin D3 secretion. PLoS Biol. *4*, e232.

Burns, C.E., Traver, D., Mayhall, E., Shepard, J.L., and Zon, L.I. (2005). Hematopoietic stem cell fate is established by the Notch-Runx pathway. Genes Dev. *19*, 2331–2342.

Carroll, K.J., Esain, V., Garnaas, M.K., Cortes, M., Dovey, M.C., Nissim, S., Frechette, G.M., Liu, S.Y., Kwan, W., Cutting, C.C., et al. (2014). Estrogen defines the dorsal-ventral limit of VEGF regulation to specify the location of the hemogenic endothelial niche. Dev. Cell *29*, 437–453.

Chen, J.K., Taipale, J., Young, K.E., Maiti, T., and Beachy, P.A. (2002). Small molecule modulation of Smoothened activity. Proc. Natl. Acad. Sci. USA *99*, 14071–14076.

Corcoran, R.B., and Scott, M.P. (2006). Oxysterols stimulate Sonic hedgehog signal transduction and proliferation of medulloblastoma cells. Proc. Natl. Acad. Sci. USA *103*, 8408–8413.

Craig, T.A., Sommer, S., Sussman, C.R., Grande, J.P., and Kumar, R. (2008). Expression and regulation of the vitamin D receptor in the zebrafish, *Danio rerio*. J. Bone Miner. Res. *23*, 1486–1496.

Dzierzak, E., and Medvinsky, A. (2008). The discovery of a source of adult hematopoietic cells in the embryo. Development *135*, 2343–2346.

Gering, M., and Patient, R. (2005). Hedgehog signaling is required for adult blood stem cell formation in zebrafish embryos. Dev. Cell *8*, 389–400.

Jao, L.-E., Wente, S.R., and Chen, W. (2013). Efficient multiplex biallelic zebrafish genome editing using a CRISPR nuclease system. Proc. Natl. Acad. Sci. USA *110*, 13904–13909.

Jeanson, N.T., and Scadden, D.T. (2010). Vitamin D receptor deletion leads to increased hematopoietic stem and progenitor cells residing in the spleen. Blood *116*, 4126–4129.

Kikuchi, K., Holdway, J.E., Major, R.J., Blum, N., Dahn, R.D., Begemann, G., and Poss, K.D. (2011). Retinoic acid production by endocardium and epicardium is an injury response essential for zebrafish heart regeneration. Dev. Cell *20*, 397–404.

Kim, P.G., Albacker, C.E., Lu, Y.-F., Jang, I.-H., Lim, Y., Heffner, G.C., Arora, N., Bowman, T.V., Lin, M.I., Lensch, M.W., et al. (2013). Signaling axis involving Hedgehog, Notch, and Scl promotes the embryonic endothelial-to-hematopoietic transition. Proc. Natl. Acad. Sci. USA *110*, E141–E150.

Kissa, K., and Herbomel, P. (2010). Blood stem cells emerge from aortic endothelium by a novel type of cell transition. Nature *464*, 112–115.

Koide, T., Hayata, T., and Cho, K.W.Y. (2006). Negative regulation of Hedgehog signaling by the cholesterogenic enzyme 7-dehydrocholesterol reductase. Development *133*, 2395–2405.

Kongsbak, M., Levring, T.B., Geisler, C., and von Essen, M.R. (2013). The vitamin d receptor and T cell function. Front. Immunol. *4*, 148.

Lam, E.Y.N., Chau, J.Y.M., Kalev-Zylinska, M.L., Fountaine, T.M., Mead, R.S., Hall, C.J., Crosier, P.S., Crosier, K.E., and Flores, M.V. (2009). Zebrafish runx1 promoter-EGFP transgenics mark discrete sites of definitive blood progenitors. Blood *113*, 1241–1249.

Lawson, N.D., Vogel, A.M., and Weinstein, B.M. (2002). sonic hedgehog and vascular endothelial growth factor act upstream of the Notch pathway during arterial endothelial differentiation. Dev. Cell *3*, 127–136.

Lin, C.-H., Su, C.-H., Tseng, D.-Y., Ding, F.-C., and Hwang, P.-P. (2012). Action of vitamin D and the receptor, VDRa, in calcium handling in zebrafish (*Danio rerio*). PLoS ONE *7*, e45650.

Lock, E.-J., Waagbø, R., Wendelaar Bonga, S., and Flik, G. (2010). The significance of vitamin D for fish: a review. Aquaculture Nutr. *16*, 100–116.

Nachtergaele, S., Mydock, L.K., Krishnan, K., Rammohan, J., Schlesinger, P.H., Covey, D.F., and Rohatgi, R. (2012). Oxysterols are allosteric activators of the oncoprotein Smoothened. Nat. Chem. Biol. *8*, 211–220.

Nedelcu, D., Liu, J., Xu, Y., Jao, C., and Salic, A. (2013). Oxysterol binding to the extracellular domain of Smoothened in Hedgehog signaling. Nat. Chem. Biol. *9*, 557–564.

Norman, A.W. (2006). Minireview: vitamin D receptor: new assignments for an already busy receptor. Endocrinology *147*, 5542–5548.

North, T.E., de Bruijn, M.F.T.R., Stacy, T., Talebian, L., Lind, E., Robin, C., Binder, M., Dzierzak, E., and Speck, N.A. (2002). Runx1 expression marks long-term repopulating hematopoietic stem cells in the midgestation mouse embryo. Immunity *16*, 661–672.

North, T.E., Goessling, W., Walkley, C.R., Lengerke, C., Kopani, K.R., Lord, A.M., Weber, G.J., Bowman, T.V., Jang, I.-H., Grosser, T., et al. (2007). Prostaglandin E2 regulates vertebrate haematopoietic stem cell homeostasis. Nature *447*, 1007–1011.

Parsons, M.J., Pisharath, H., Yusuff, S., Moore, J.C., Siekmann, A.F., Lawson, N., and Leach, S.D. (2009). Notch-responsive cells initiate the secondary transition in larval zebrafish pancreas. Mech. Dev. *126*, 898–912.

Plum, L.A., and DeLuca, H.F. (2010). Vitamin D, disease and therapeutic opportunities. Nat. Rev. Drug Discov. *9*, 941–955.

Schwend, T., Loucks, E.J., and Ahlgren, S.C. (2010). Visualization of Gli activity in craniofacial tissues of hedgehog-pathway reporter transgenic zebrafish. PLoS ONE *5*, e14396.

Tang, J.Y., Xiao, T.Z., Oda, Y., Chang, K.S., Shpall, E., Wu, A., So, P.-L., Hebert, J., Bikle, D., and Epstein, E.H., Jr. (2011). Vitamin D3 inhibits hedgehog signaling and proliferation in murine Basal cell carcinomas. Cancer Prev. Res. (Phila.) *4*, 744–751.

Yetgin, S., Ozsoylu, S., Ruacan, S., Tekinalp, G., and Sarialioğlu, F. (1989). Vitamin D-deficiency rickets and myelofibrosis. J. Pediatr. *114*, 213–217.

Zhu, H., Traver, D., Davidson, A.J., Dibiase, A., Thisse, C., Thisse, B., Nimer, S., and Zon, L.I. (2005). Regulation of the lmo2 promoter during hematopoietic and vascular development in zebrafish. Dev. Biol. *281*, 256–269.

Stem Cell Reports, Volume *5*

Supplemental Information

Accumulation of the Vitamin D Precursor Cholecalciferol Antagonizes Hedgehog Signaling to Impair Hemogenic Endothelium Formation

Mauricio Cortes, Sarah Y. Liu, Wanda Kwan, Kristen Alexa, Wolfram Goessling, and Trista E. North

Gene	Primers	
PPARγ	S	5'-ATGTAAGTGGATATTGAATAGTTTTTGTTTTG-3'
	AS	5'-CCCATAAATCAAAACATCAATTTCC-3'
UCP1	S	5'-GGAGAGGAAAGGGAAGTAGAGAA-3'
	AS	5'-CCCTCCCATTCCCATTCTCGCTCG-3'

Supplementary Table S1 (Related to Figure 4). PCR primers for bisulfite sequencing are shown. See also Figure 4.

sh*Ucp1* 280	Sense	5'-GATCCGATCTTCTCAGCCGGAGTTTCCTCGAGGAAACTCCGGCTGAGAAGATCTTTTTG-3'
	Antisense	5'-AATTCAAAAAGATCTTCTCAGCCGGAGTTTCCTCGAGGAAACTCCGGCTGAGAAGATCG-3'

sh*Ucp1* 666	Sense	5'-GATCCGCCATCTGCATGGGATCAAACCTCGAGGTTTGATCCCATGCAGATGGCTTTTTG-3'
	Antisense	5'-AATTCAAAAAGCCATCTGCATGGGATCAAACCTCGAGGTTTGATCCCATGCAGATGGCG-3'

sh*Ucp1* 1068	Sense	5'-GATCCGGTCCTGGAACGTCATCATGTCTCGAGACATGATGACGTTCCAGGACCTTTTTG-3'
	Antisense	5'-AATTCAAAAAGGTCCTGGAACGTCATCATGTCTCGAGACATGATGACGTTCCAGGACCG-3'

Supplementary Table S2 (Related to Figure 7). Sequences of sh*Ucp1*. See also Figure 7.

Supplementary Figure S1

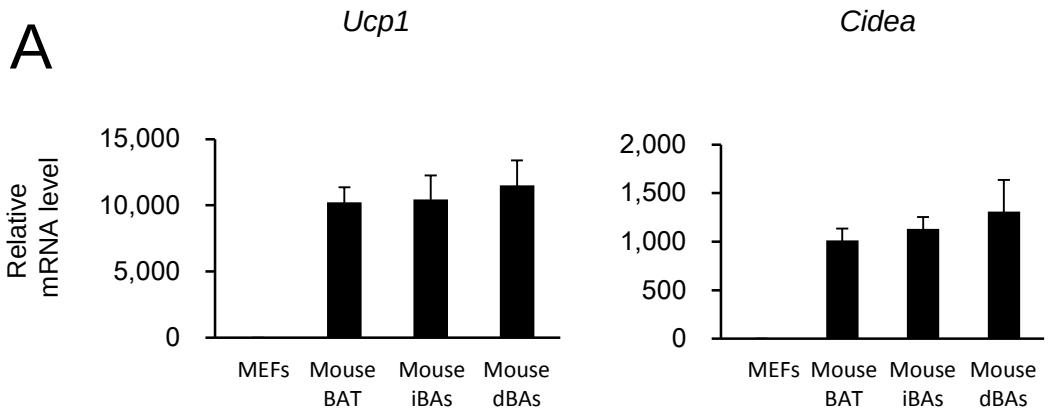

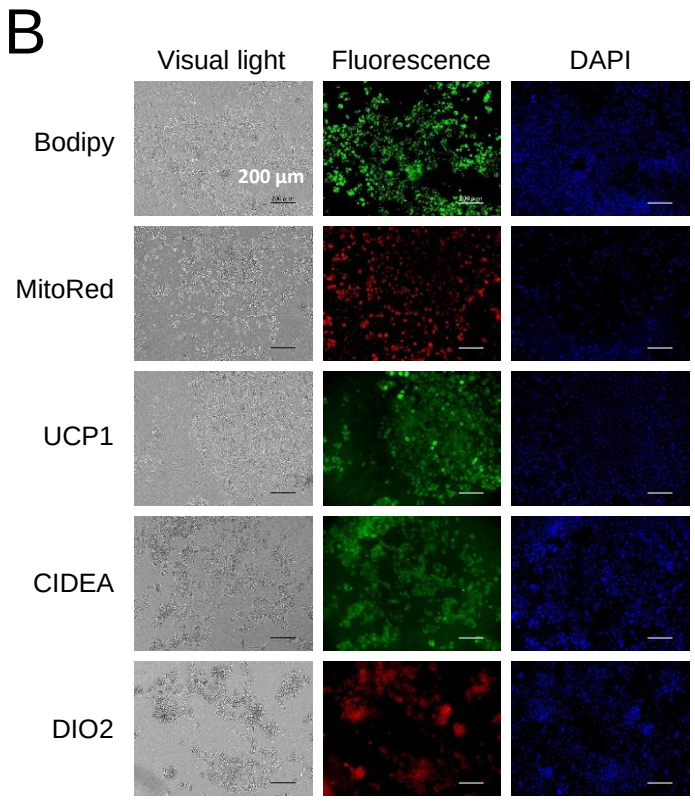

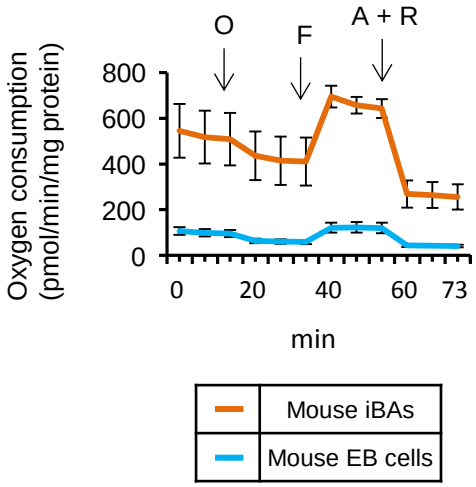

Supplemental Figure S1

Characterization of mouse iBAs (Related to Figure 2). **A**, Mouse iBAs were induced from the iPS cell-derived embryoid body cells by transducing *Prdm16* gene and subsequently culturing for 12 days as described in the Experimental Procedures. Mouse dBAs were induced from MEFs by transducing *PCL* retrovirus vectors and subsequently culturing for 12 days. RNA was extracted from these cells and from the mouse brown adipose tissue (BAT), and real time-RT-PCR analysis was performed using primers/probes specific for *Ucp1* and *Cidea* genes. Values (average ± s.d.) were normalized to *β-Actin* mRNA and expressed relative to values for the MEFs (set to 1.0)(*n*=3 cultures per group). **B**, Mouse iBAs were stained with Bodipy 493/503 (Top) and Mitotracker Red (Second to the top) to visualize lipid droplets and mitochondria, respectively. Other aliquots of cells were incubated with anti-UCP-1, anti-CIDEA and anti-DIO2 antibodies, followed by staining with secondary antibodies. Cell nuclei were also stained with DAPI. Original magnification was x100. **C**, Oxygen consumption of mouse iBAs and embryoid body (EB) cells (average ± s.d.) was evaluated as in Fig. 1E (*n*=3 cultures per group).

Supplementary Figure S2

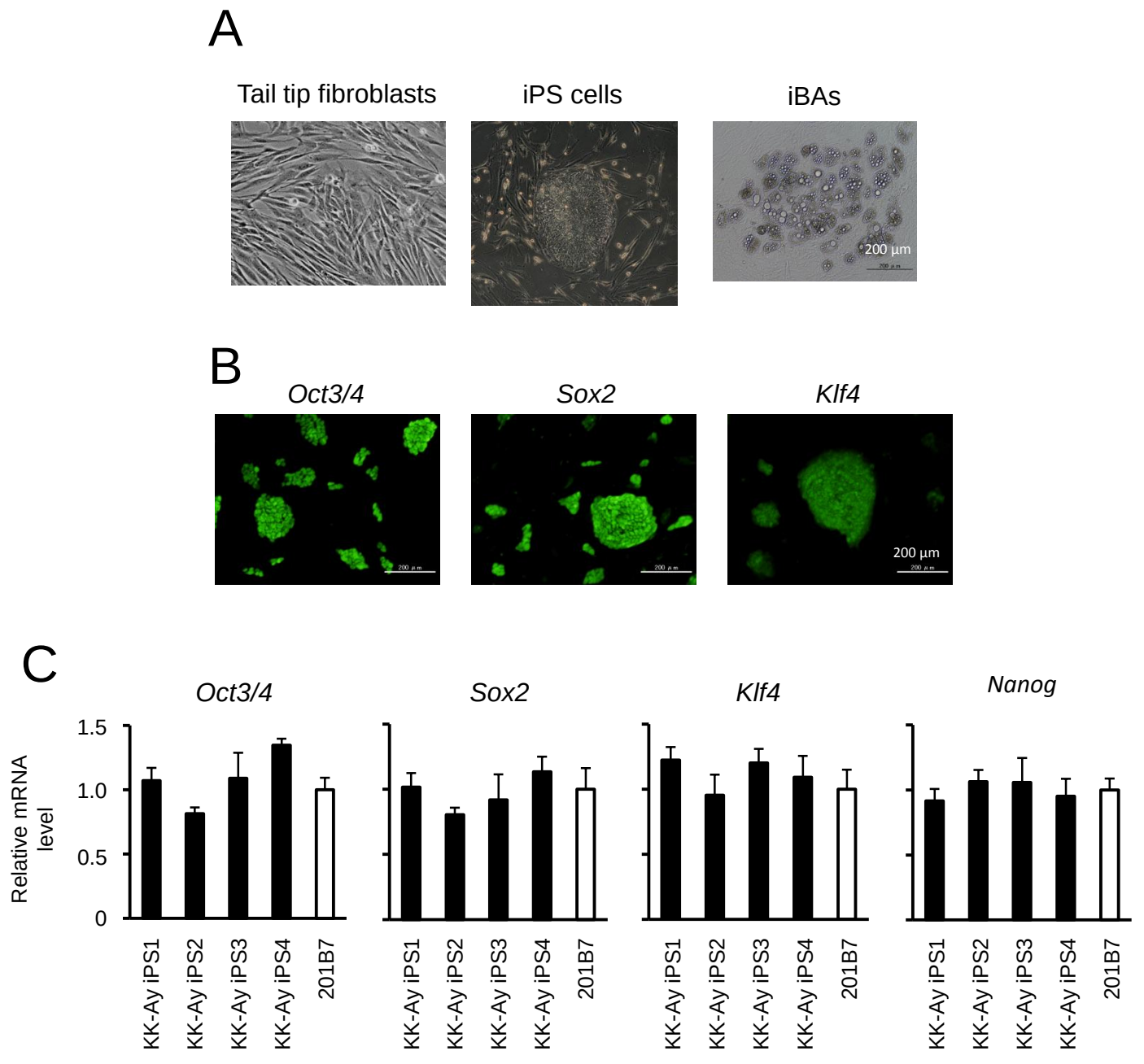

Supplemental Figure S2
iPS cells induced from KK-Ay diabetic mice (Related to Figure 2). Tail tip fibroblasts were obtained from KK-Ay mice, and iPS cells were induced by transducing *Oct3/4*, *Sox2*, *Klf4* and *C-myc* retroviral vectors. iBAs were induced from the iPS cells as described in the Experimental Procedures. **A**, Phase contrast microscopic images of the cells are shown. **B**, KK-Ay iPS cells were immunostained for the indicated transcription factors. **C**, RNA was extracted from four independent iPS cell clones, and mRNA levels for the indicated genes were evaluated by real time RT-PCR. Values (average ± s.d.) were normalized to *β-Actin* mRNA and expressed relative to levels in the 201B7 mouse iPS cells (set to 1.0) (*n*=3 cultures per group).

Supplementary Figure S3

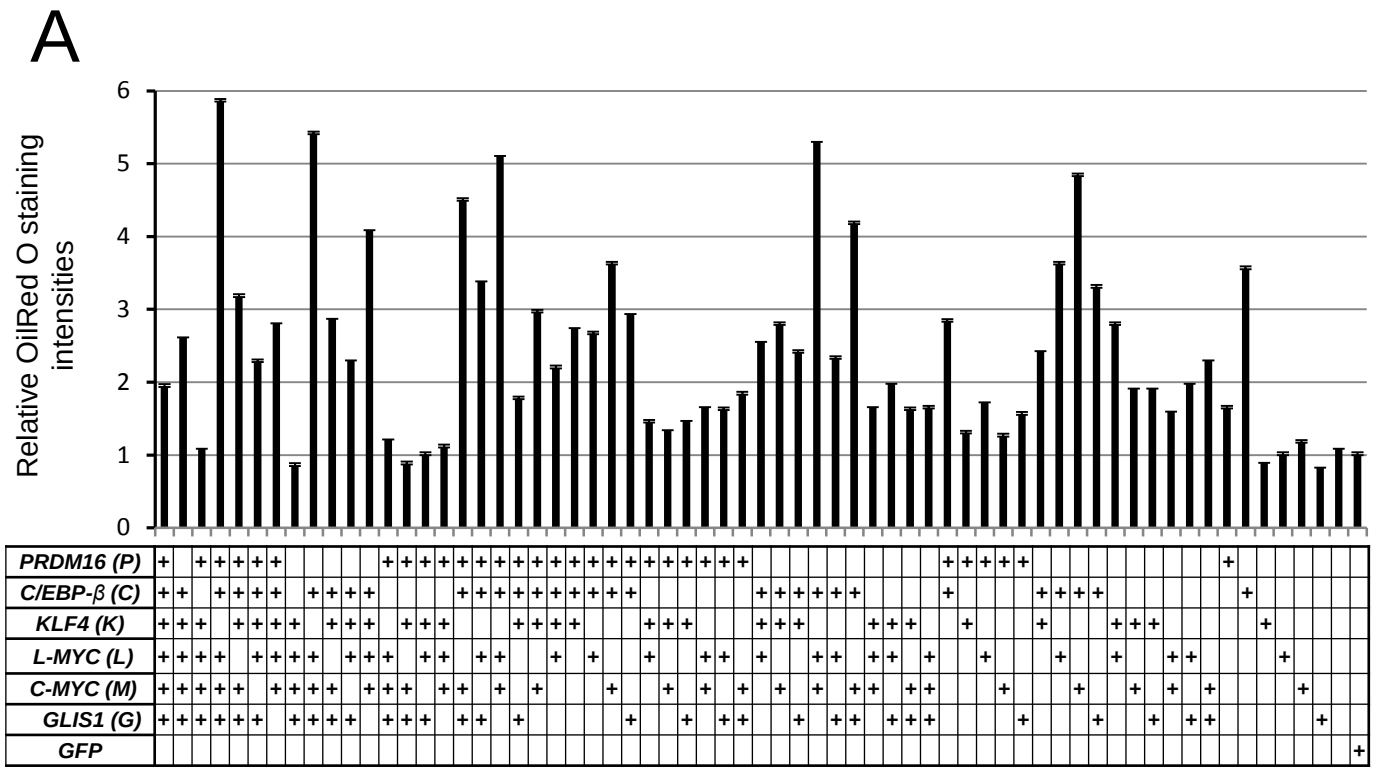

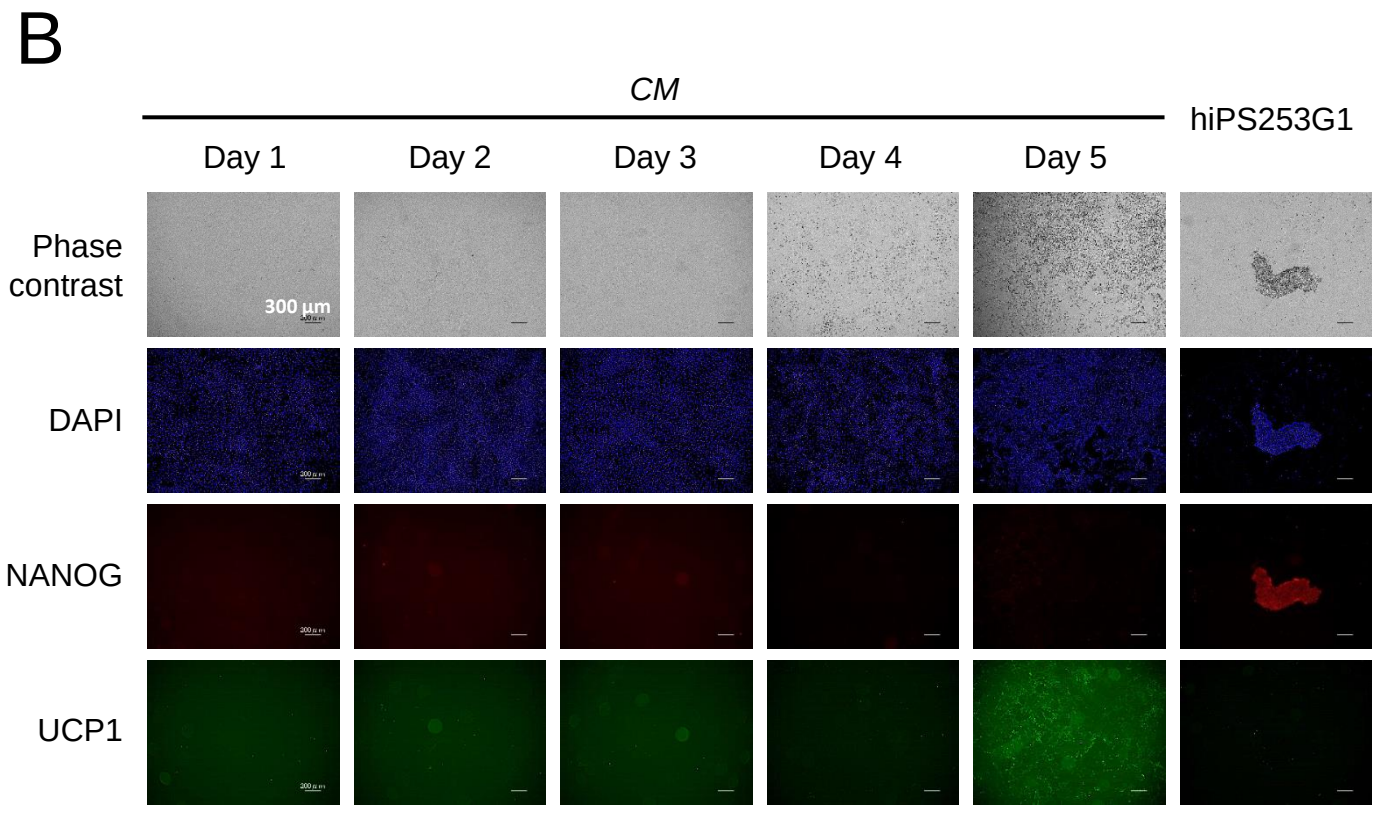

Supplemental Figure S3

Direct conversion of normal human fibroblasts into BAs (Related to Figure 3). **A**, HDFs were seeded into 12-well plate and transduced with mixtures of the indicated genes as described in the Methods ("+" in the Table represents the presence of the corresponding gene). After culturing for 14 days, cells were stained with Oil Red O, and OD_{550} for cell lysates was measured. Values are average ± s.d. (*n*=3 technical replicates). **B**, Human fibroblasts were transduced with *CM* retroviral vectors, and the indicated days later, nuclear staining with DAPI as well as immunostaining with anti-NANOG (cat, RCAB0003P; Repro Cell Inc.) and anti-UCP1 (cat, PAB6905; Abnoba) antibodies were performed. Human iPS cells were also stained as a NANOG-positive control (the rightmost panels). Immunostaining images were obtained using haze reduction. No detectable level of NANOG was demonstrated in fibroblasts between 1 to 5 days after the transduction, while UCP1 was significantly expressed on day 5, indicating that the dBAs were induced from normal fibroblasts without passing a pluripotent stage (*n*=5 cultures per group).

Supplementary Figure S4

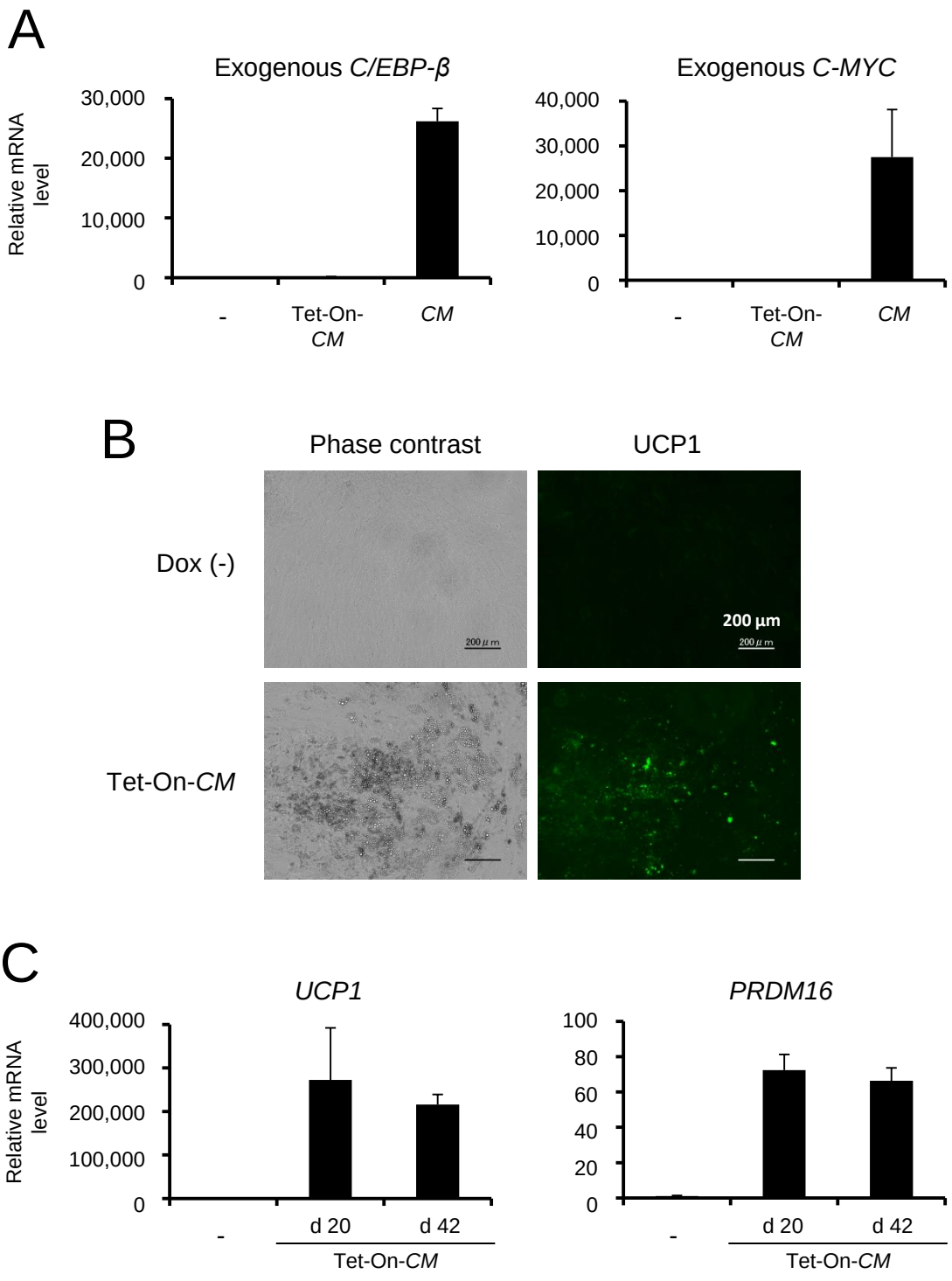

Supplemental Figure S4

Continuous expression of exogenous *C/EBP-β* and *c-Myc* genes may not be essential for dBAs to maintain the BA phenotype (Related to Figure 3). **A**, Human dermal fibroblasts were transduced with retrovirus vectors containing *C* and *M* genes driven by Tet-On promoter (Tet-On-*CM*)(day 0). Cells were cultured as in Figure 3, except that doxycyclin was added to the culture only during the first 20 days. On day 42 colonies with lipid droplets were picked up, and mRNA levels for the retroviral transgenes were evaluated by real time RT-PCR. Non-transduced cells (-) were analyzed as negative control. The cells transduced with conventional *CM* that constitutively expressed *C/EBP-β* and *C-MYC* genes were also analyzed on day 42 as positive control. **B**, Fibroblasts were transduced with Tet-On-*CM* and cultured as in (A). An aliquot of cells were transduced with Tet-On-*CM* and cultured without doxycyclin as control (Dox (-)). On day 42, cells were immuno-stained by anti-UCP1 antibody. Phase contrast and green fluorescence images are shown (magnification, x 100). **C**, Fibroblasts were transduced with Tet-On-*CM* and cultured with doxycycline (days 0-20) and without doxycyclin (days 21-42) as in (A). On days 20 and 42, colonies with lipid droplets were picked up, and mRNA levels for the indicated genes were evaluated. In (A) and (C), values (average ± s.d.) were normalized to *β-ACTIN* mRNA and expressed relative to levels in the non-transduced fibroblasts (set to 1.0) (*n*=3 cultures per group).

Supplementary Figure S5

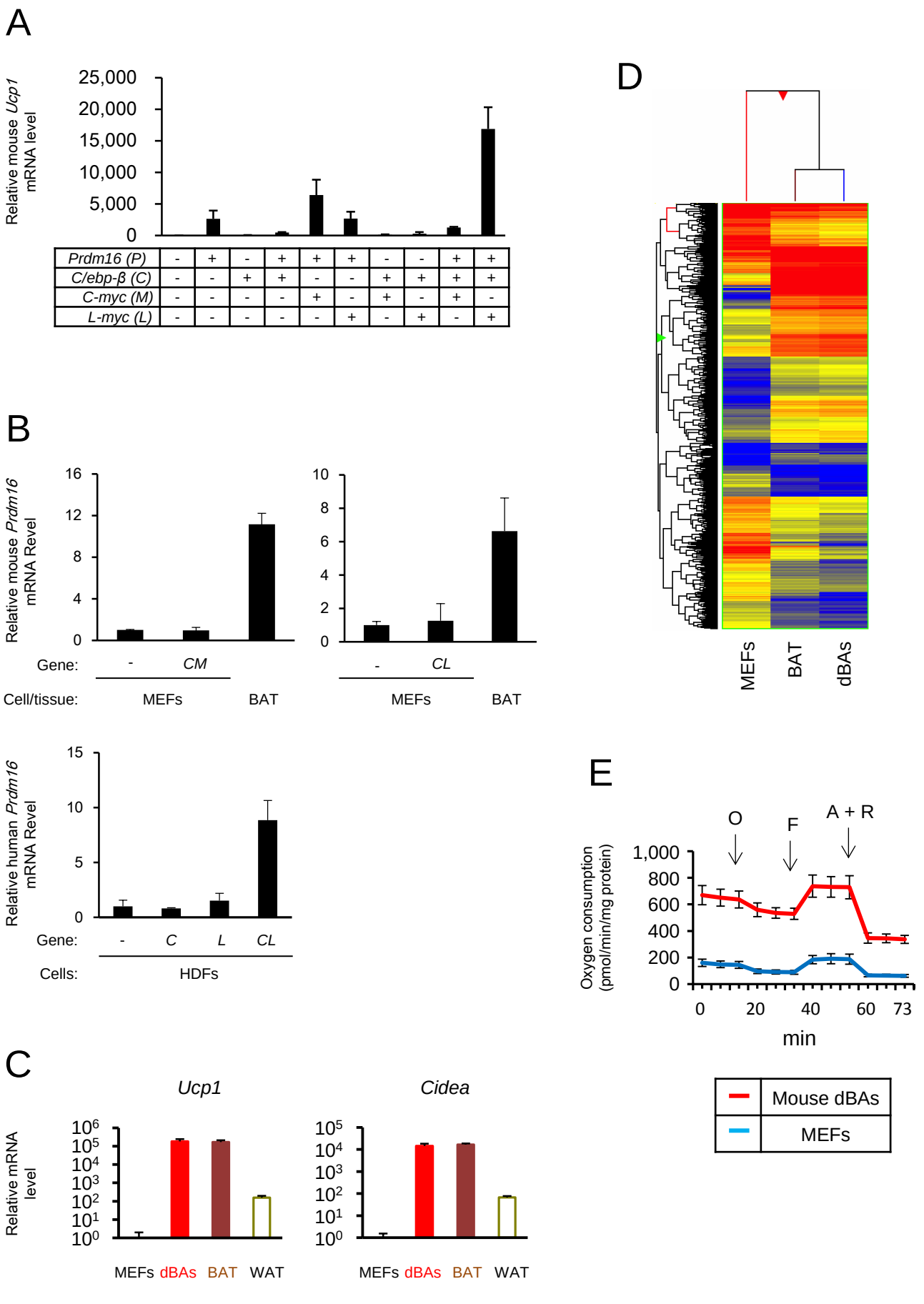

Supplemental Figure S5

Characterization of mouse dBAs (Related to Figure 6). **A**, Mouse fibroblasts were converted into dBAs by transduction with *PCL*. Mouse embryonal fibroblasts (MEFs) were transduced with the indicated retroviral vectors ("+" in the Table represents the presence of the corresponding gene). After culturing for 12 days, *Ucp1* and *β-Actin* mRNA was evaluated by real time RT-PCR. *Ucp1* mRNA levels (average ± s.d.) were normalized to *β-Actin* mRNA and expressed relative to levels in the untransduced MEFs (set to 1.0) (*n*=3 cultures per group). **B**, *Prdm16* mRNA was not induced in mouse fibroblasts by *CM* or *CL* transduction. MEFs (Upper) or HDFs (Lower) were transduced with the indicated retrovirus vectors, and subsequently cultured for 12 days as in (A). RNA was extracted from the cells and real time-RT-PCR was performed to evaluate the mRNA levels of the mouse (Upper) and human (Lower) *PRDM16* genes. As control, RNA extracted from non-transduced fibroblasts and brown adipose tissue (BAT) of mice was also tested. Values (average ± s.d.) were normalized to *β-Actin* mRNA and expressed relative to values for the MEFs (set to 1.0)(*n*=3 cultures per group). The mouse fibroblasts did not significantly express *Prdm16* mRNA after *CM* or *CL* transduction, which was in sharp contrast to human fibroblasts that were provoked to express *PRDM16* mRNA by *CM* or *CL* transduction. This may explain why exogenous *Prdm16* gene is required for direct conversion of mouse fibroblasts into BAs. The transduction of *CL* induced human fibroblasts to express *PRDM16* mRNA at a lower level than *CM* transduction, which may be the reason why *CM* was superior to *CL* in converting human fibroblasts into BAs (Figure S3A). **C**, Mouse dBAs expressed BA markers at high levels. MEFs were transduced with *PCL* retroviral vectors as in (B). After culturing for 12 days, RNA was extracted from the dBAs as well as untransduced MEFs, mouse brown and white adipose tissues (BAT and WAT, respectively). *Ucp1*, *Cidea* and *β-Actin* mRNA was evaluated by real time RT-PCR. Shown are *β-Actin*-normalized *Ucp1* and *Cidea* mRNA levels in each sample (average ± s.d.) relative to those in the untransduced MEFs (set to 1.0) (*n*=3 cultures per group). **D**, Mouse dBAs showed similar gene expression profiles as BAT. MEFs were transduced with *PCL* retroviral vectors as in (B). Twelve days later RNA was extracted from the cells. RNA was also extracted from BAT and untransduced MEFs. DNA microarray analysis demonstrated that among 28,853 genes tested, 4,644 genes were differentially expressed (>2 folds). Heat map and hierarchical clustering analysis of the genes are shown. Red and blue colorations indicate increased and decreased expression, respectively. **E**, Oxygen consumption of the indicated cells (average ± s.d.) was evaluated as in Fig. 1E (*n*=3 cultures per group).

Supplementary Figure S6

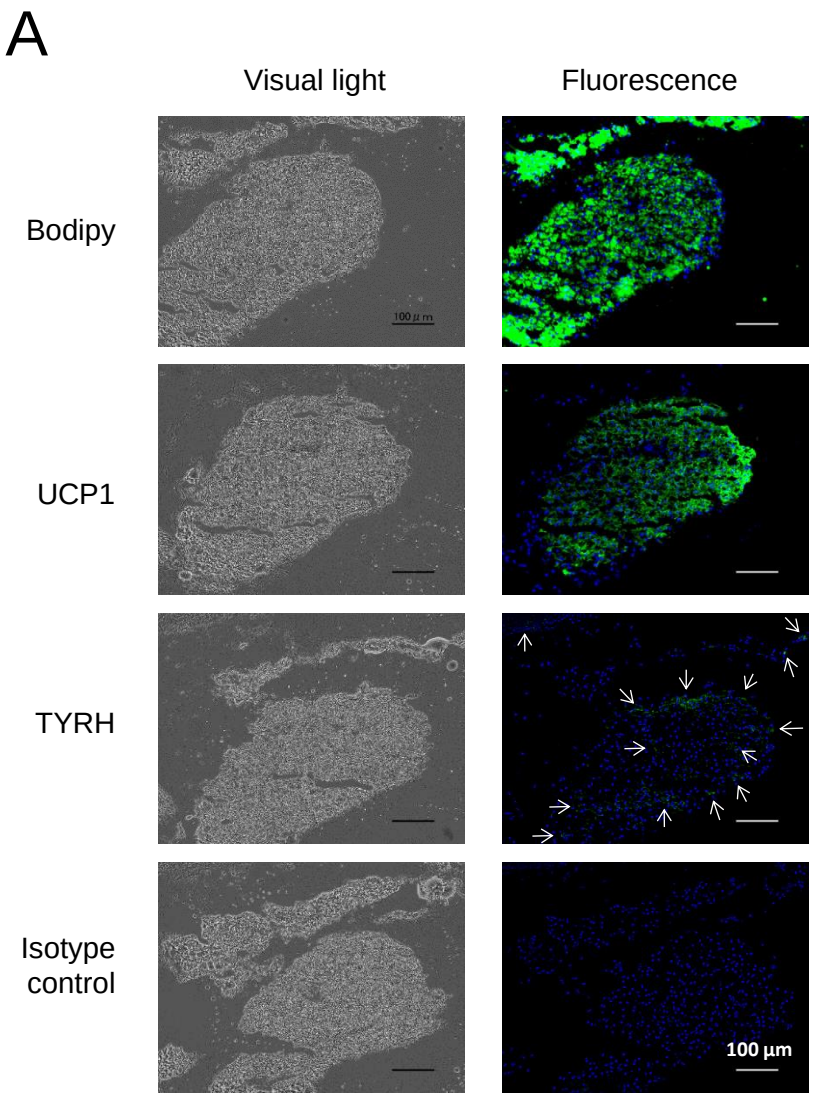

Supplemental Figure S6

Sympathetic innervation in BA graft, and siRNA-mediated silencing of *UCP1* (Related to Figures 6 and 7). **A**, Mouse dBAs were subcutaneously transplanted into syngenic mice as in Figure 6. Twelve days later, mice were sacrificed and graft tissue was excised. Cryosections were stained with Bodipy 493/503 to visualize lipid droplet (Top). Other sections were incubated with anti-UCP1 (R&D Systems, cat no. MAB6158), anti-tyrosine hydroxylase (TYRH)(ImmunoStar, cat no. 22941) and isotype-matched control antibodies, followed by staining with a CF488-conjugated anti-mouse IgG secondary antibody (Biotium, cat no. 20014). The sections were also stained with DAPI to visualize cell nuclei. TYRH-positive cells are indicated by arrows. (Original magnification was x 200). **B**, KK-Ay tail tip fibroblasts were transduced with three different *Ucp1*-specific shRNA via lentiviral vectors. sh*Ucp1* 280, 666 and 1068 sequences (see Supplemental Table S2) were inserted into pGreen puro vector (SBI System Biosciences), and co-transfected into 293TN packaging cells with pCMV-VSV-G, pPACKH1-GAG and pPACKH1-REV plasmids using X-treme Gene 9 transfection reagent (Roche Applied Science). Twenty-four hours later culture medium was replaced by fresh antibiotic-free medium, and after another 24 hours of culturing, supernatant was harvested, filtrated through a 0.45 um pore size filter and used for infection. Five days later, *Ucp1* and *β-Actin* mRNA levels were evaluated by real time-RT-PCR. *Ucp1* mRNA levels (average ± s.d.) were normalized to *β-Actin* mRNA and expressed relative to levels of the non-transduced cells (set to 1.0) (*n*=3 cultures per group). The sh*Ucp1* 1028 reduced *Ucp1* mRNA level by 86%, and were used in the experiments shown in Fig. 7.

Supplementary Figure S7

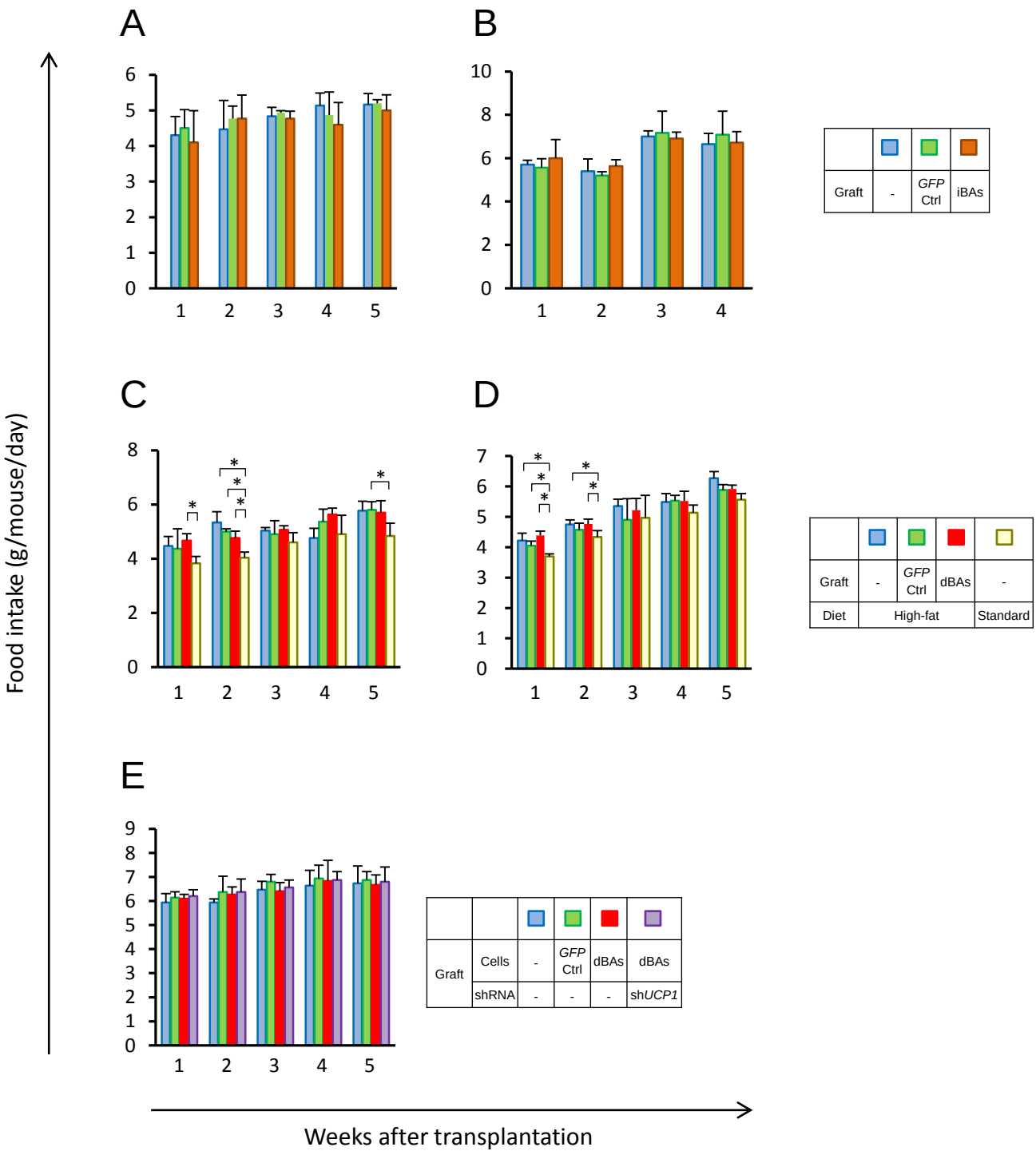

Supplemental Figure S7
Food intake of mice (Related to Experimental Procedures). In the experiments shown in Figs. 2C (A), 2E (B), 6A (C), 6C (D) and 7A (E), food intake of the mice in each group was calculated weekly. Values are average +/- S.D. (*n*=3 (A, B, D and E) and 5 (C) mice per group). In C and D, some mouse groups that were fed the high-fat diet consumed significantly more food than the mice fed a standard chow at some points (*P < 0.05, two-sided Student's t test). But no significant difference was seen among the food consumption of the mouse groups fed high-fat diet, strongly suggesting that the suppression of body weight gain by BA transplantation (Figs. 2C, 2E, 6A, and 7A) was not due to different dietary intake.